

RESEARCH ARTICLE | OCTOBER 18 2023

## Optothermal crystallization of hard spheres in an effective bidimensional geometry

Vincenzo Ruzzi  ; Jacopo Baglioni  ; Roberto Piazza  



*J. Chem. Phys.* 159, 154904 (2023)

<https://doi.org/10.1063/5.0169221>



View  
Online



Export  
Citation

CrossMark

### Articles You May Be Interested In

Signal processing in optothermal spectroscopy

*Journal of Applied Physics* (May 1986)

Optothermal transport behavior in whispering gallery mode optical cavities

*Appl. Phys. Lett.* (August 2014)

Calibration of optothermal stratum corneum hydration measurements

*Rev Sci Instrum* (January 2003)

500 kHz or 8.5 GHz?  
And all the ranges in between.

Lock-in Amplifiers for your periodic signal measurements



Find out more

 Zurich  
Instruments

# Optothermal crystallization of hard spheres in an effective bidimensional geometry

Cite as: J. Chem. Phys. 159, 154904 (2023); doi: 10.1063/5.0169221

Submitted: 24 July 2023 • Accepted: 1 October 2023 •

Published Online: 18 October 2023



View Online



Export Citation



CrossMark

Vincenzo Ruzzi,  Jacopo Baglioni,<sup>a)</sup>  and Roberto Piazza<sup>b)</sup> 

## AFFILIATIONS

Department of Chemistry, Materials Science, and Chemical Engineering (CMIC) “Giulio Natta,” Politecnico di Milano, Edificio 6, Piazza Leonardo da Vinci 32, 20133 Milano, Italy

<sup>a)</sup>Current address: Department of Physics and Astronomy, Via F. Marzolo 8, 35131 Padova, Italy.

<sup>b)</sup>Author to whom correspondence should be addressed: [roberto.piazza@polimi.it](mailto:roberto.piazza@polimi.it)

## ABSTRACT

Using colloids effectively confined in two dimensions by a cell with a thickness comparable to the particle size, we investigate the nucleation and growth of crystallites induced by locally heating the solvent with a near-infrared laser beam. The particles, which are “thermophilic,” move towards the laser spot solely because of thermophoresis with no convection effects, forming dense clusters whose structure is monitored using two order parameters that gauge the local density and the orientational ordering. We find that ordering takes place when the cluster reaches an average surface density that is still below the upper equilibrium limit for the fluid phase of hard disks, meaning that we do not detect any sign of a proper “two-stage” nucleation from a glass or a polymorphic crystal structure. The crystal obtained at late growth stage displays a remarkable uniformity with a negligible amount of defects, arguably because the incoming particles diffuse, bounce, and displace other particles before settling at the crystal interface. This “fluidization” of the outer crystal edge may resemble the surface enhanced mobility giving rise to ultra-stable glasses by physical vapor deposition.

© 2023 Author(s). All article content, except where otherwise noted, is licensed under a Creative Commons Attribution (CC BY) license (<http://creativecommons.org/licenses/by/4.0/>). <https://doi.org/10.1063/5.0169221>

## I. INTRODUCTION

Developing efficient strategies for assembling two-dimensional colloidal crystals are of paramount importance in many advanced technology applications, ranging from photonic crystal optics<sup>1</sup> to nanosphere lithography.<sup>2</sup> However, 2D systems notoriously display a very peculiar phase behaviour,<sup>3</sup> with some still debated features, and many issues concerning the crystallization kinetics of 2D colloidal suspensions still deserve further investigation.<sup>4</sup> In this paper we focus on the nucleation and growth of crystals of hard spheres confined in two dimensions, showing that particle thermophoresis can profitably be exploited to obtain high-quality 2D crystals.

A solid experimental evidence suggests that the pathway to crystallization is far more involved, both in simple and complex fluids, than predicted by classical homogeneous nucleation theory.<sup>5–7</sup> Such a rich scenery is substantiated by computer simulations that bring to light the key role played by fluctuations

in generating dense clusters acting as precursor of the ordered phase.<sup>8</sup> A huge enhancement of the nucleation rate due to the critical fluctuations associated with the presence of a metastable gas–liquid phase boundary was originally suggested for molecular or colloidal systems such as globular proteins interacting via a short-ranged attractive potential.<sup>9</sup> Perhaps more surprising is that structural precursors to freezing have been predicted even for hard spheres from the behavior of the radial distribution function close to freezing,<sup>10</sup> clearly detected in simulations,<sup>11</sup> and invoked to account for light scattering experiments on colloids,<sup>12</sup> although extracting unquestionable evidence of multi-step nucleation processes from bulk scattering experiment is not trivial at all. The physical nature of these “precursors” have recently been unraveled in accurate simulations by Wöhler and Schilling<sup>13</sup> suggesting that they consist of assemblies of polymorphic microcrystals, an observation that may even explain the huge divergence between simulation and experimental results for hard sphere nucleation rates.

With respect to 3D studies, direct visualization of 2D colloidal monolayers, which easily allows telling ordered crystal-lites from amorphous clusters or spotting crystal defects, offers for sure several advantages. Crystal nucleation can be induced even for dilute suspension by introducing attractive interparticle interactions via the addition of a depletion agent. This strategy has successfully been adopted by Savage and Dinsmore<sup>14</sup> to highlight two-step nucleation processes in suspensions by adding nonionic surfactant micelles inducing depletion forces whose strength increases with temperature.<sup>15</sup> In purely repulsive systems, 2D crystal monolayers can be obtained by using thermosensitive microgel particles, whose size can be tuned by changing temperature. This strategy has been successfully used to investigate 2D-crystal melting in experiments that clearly showed the occurrence of an intermediate hexatic phase between the ordered and the fluid phase.<sup>16</sup> This approach, however, in which the initial condition is that of a dense fluids, is not particularly suited to detect the occurrence of amorphous cluster forerunning crystal ordering.

An interesting alternative approach is investigating how a *single* dense cluster created by the application of an external field acts as a seed for heterogeneous crystal nucleation.<sup>17</sup> On the experimental side, this is most efficiently done in a 2D geometry. Unfortunately, in most investigations exploiting such a strategy, colloidal particles just settle by sedimentation forming a planar monolayer in a cell having a significant vertical extent. With such an arrangement, any minimal horizontal density, composition, or temperature gradient will induce natural convection, which usually is the true, hardly quantifiable driving force for particle accumulation. Besides, convection often piles up particles on more than a single surface layer, which makes the interpretation of the experimental observations harder. Complex hydrodynamic effects are likely to play a complex role even in studies where a true 2D geometry is cleverly ensured by tethering particles at a fluid–fluid interface.<sup>18</sup>

Nevertheless, claims of a two-stage nucleation have been made in several field-driven 2D crystallization experiments.<sup>19,20</sup> This evidence is however quite surprising, since, at variance with hard spheres, for hard disks no crystal polymorphism exists that may account for clusters packed at surface densities  $\varphi$  larger than the upper limit ( $\varphi \simeq 0.7$ ) for the fluid phase. Moreover, as for monodisperse hard spheres, no dynamically arrested glass is expected for hard disks, although in principle one may conceive the occurrence of long-lived metastable disordered structures denser than the fluid freezing limit. The fact is, no explicit evaluation of the surface density of the precursor has, to our knowledge, been presented.

In this work, by effectively confining hard-sphere colloids in thin cells where particle convection cannot take place, we monitor as a function of the initial particle surface coverage and of the strength of an applied optothermal field the accumulation of particles by thermophoresis, assessing the growth of the local surface density and order parameters in the cluster and quantifying the conditions required for crystallization. We then follow the growth kinetics of the nucleus, pointing out and trying to explain the remarkable uniformity of the large 2D crystals obtained at late stage. By turning off the optothermal field we finally quantitatively assess the increase of disorder upon crystal melting by following

the time evolution of the Voronoi tessellation of the system, finding that in a dense fluid the distribution of the coordination number of a particle, defined as the number of vertices of the associated Voronoi cell, is very narrow, in agreement with the simulation results.

## II. EXPERIMENTAL SETUP AND METHODS

### A. Colloidal system and 2D cell

We have investigated aqueous colloids of monodisperse silica particles (Microparticles<sup>®</sup> GmbH) with a radius  $a = 2.0 \pm 0.05 \mu\text{m}$ , confined in a cell consisting of two carefully cleaned and plasma-treated microscope coverslips, glued together by two strips of a double-side tape (Nitto-Denko Corp., Japan, No. 5600) made of a polyester film, ensuring rigidity and thickness uniformity, sandwiched between two acrylic adhesive layers. This ultrathin tape fixes the coverslip separation to  $h = 5 \mu\text{m}$  with an accuracy better than 10%. The original particle batch, at a concentration  $c = 5\%$  in weight, is diluted in distilled water to a particle volume fraction  $\Phi$ , yielding a nominal surface coverage  $\varphi_0 = (3h/4a)\Phi = \pi a^2 h n$ , where  $n$  particle number density that we varied in the range  $3 \times 10^{-3} \leq \varphi_0 \leq 0.25$ , which is then carefully adjusted by microscope imaging. Samples are then fed in the gap between the coverslips from a lateral side by capillarity. The lateral sides are finally covered with a thin layer of CoverGrip<sup>™</sup> to make the assembly gas-tight over days, and the cell is placed on the three-axes tilting stage of a custom-built microscope station equipped with a high precision inclinometer (WitMotion WT901) allowing the cell to be set horizontally with high accuracy to minimize any drift due to particle settling. A sketch of the cell assembly is shown in Fig. 1. Since the particle gravitational length  $\ell_g \simeq 12 \text{ nm} \ll a$ , all particles lie on the cell bottom, leaving a  $1 \mu\text{m}$  free solvent layer at the top, too thin to allow for particle convection.

### B. Optical setup and image analysis

The optical setup, shown in Fig. 1, is derived from a Modular Tweezers module (Thorlabs) based on an inverted microscope using a EPlan Nikon 10 $\times$  objective (NA = 0.25) and a Olympus 10 $\times$  (NA = 0.3) condenser. The microscope is equipped with a fluorescence module with a tunable green LED (central wavelength  $\lambda = 565 \text{ nm}$ , Thorlabs M565L3) and a set of excitation, emission, and dichroic filters for rhodamine. Optical heating is provided by a butterfly laser diode emitting in a Gaussian mode at  $1.44 \mu\text{m}$ , where water has an absorption coefficient  $b \simeq 31 \text{ cm}^{-1}$ .<sup>21</sup> The infrared (IR) beam propagates in a single-mode fiber, is then collimated by a triplet lens with a focal length of 6.15 mm and a numerical aperture of 0.28, and is finally focused on the sample plane with a spot size (diameter)  $w \simeq 40 \mu\text{m}$ .

The imaging optics yields a field-of-view of  $480 \times 600 \mu\text{m}^2$ , corresponding to almost  $2 \times 10^4$  times a particle sectional area. Images are collected by a  $1280 \times 1024 \text{ px}$ . CMOS color camera (Thorlabs DCC1240C) placed along the transmitted illumination path, and acquired at a frame rate varying between 1 and 11.5 fps depending on the strength of the imposed thermal gradient. Red-green-blue (RGB) images are then converted in 16-bit grey scale images and contrasted to lighten the particle contour. The intensity profile of the infrared

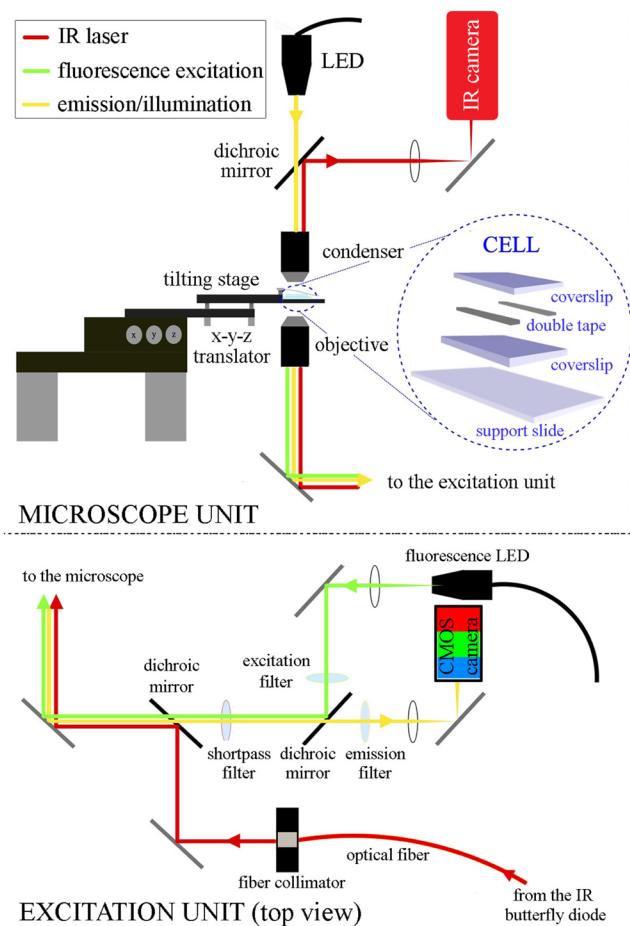


FIG. 1. Scheme of the experimental setup.

laser beam on the sample plane is obtained using a Contour IR Digital camera (Ados Tech, Latvia) based on an IR-enhanced CMOS 1/3 in. sensor with a spectral range extending up to 1700 nm.

Particle tracks are obtained using TrackMate,<sup>22</sup> a particle-tracking software running on ImageJ<sup>®</sup>. Attention must be paid to residual drifts due to sedimentation, since a cell inclination as low as  $\theta = 1^\circ$  would still lead to a settling speed of about  $0.2 \mu\text{m s}^{-1}$  superimposing to the particle thermophoretic motion (see below). Consequently, a careful correction was always performed by monitoring the particle motion before the thermal gradient is applied and subtracting out the residual drift by software.

A custom-developed algorithm, based on Matlab<sup>®</sup> *regionprops* function spots the location of particle centroids with an accuracy of about 50 nm and performs Delaunay triangulation. To avoid mistaking transient vacancies for particles in a growing crystal, the code deploys a particle-tracking section designed to work in tightly-packed structures.

### C. Fluorescence thermometry

The radial temperature profiles generated by water absorption of the IR laser are obtained by measuring the spatial distribution of

the  $T$ -dependent fluorescence intensity emitted by 1 mM aqueous solutions of rhodamine B (AAT Bioquest), a probe routinely used for non-invasive temperature measurements with an excitation wavelength  $\lambda_{exc} = 554 \text{ nm}$  and an emission wavelength  $\lambda_{em} = 575 \text{ nm}$ .<sup>23</sup> The thermal profile is evaluated from the frame acquired about 0.5 s after the IR laser is switched on, a timescale much longer than the heat diffusion time over the field of view  $\tau_{th} \approx 60 \text{ ms}$ , but still too short for any significant concentration gradient due to rhodamine thermodiffusion to build up.

## III. RESULTS

### A. Particle constrained diffusion and settling

In the absence of thermal gradients, particle tracking yields a diffusion coefficient parallel to the cell walls  $D_{\parallel} \approx 0.028 \mu\text{m}^2 \text{ s}^{-1}$  for the silica particles, a figure that is only about 27% of the Stokes–Einstein value  $D_0$ . Such a significant reduction is due to the tight vertical confinement. The effect of the proximity of a *single* hard wall on  $D_{\parallel}$  can approximately be accounted for using a series expansion in  $a/z$ , where  $z$  is the (average) distance from the center of the sphere with radius  $a$  to the wall. To fifth order, one has, for  $\gamma^1(z) = D_{\parallel}(z)/D_0$ ,<sup>24</sup>

$$\gamma^1(z) \approx 1 - \frac{9}{16} \left(\frac{a}{z}\right) + \frac{1}{8} \left(\frac{a}{z}\right)^3 - \frac{45}{256} \left(\frac{a}{z}\right)^4 - \frac{1}{16} \left(\frac{a}{z}\right)^5. \quad (1)$$

Quantitative evaluation of the effects of confinement by *two* parallel walls separated by  $h$  is notoriously much harder. Yet a simple linear superposition approximation, consisting in taking<sup>25</sup>

$$\frac{D_{\parallel}}{D_0} = \frac{1}{\gamma^1(z)^{-1} + \gamma^1(h-z)^{-1} - 1} \quad (2)$$

yields values that are in good agreement with experimental data, and has recently been shown to be very close to the result of a rigorous but extremely intricate hydrodynamic analysis. In our case we have  $\gamma^1(z) = \gamma^1(a) \approx 0.324$ ,  $\gamma^1(h-z) = \gamma^1(3a/2) \approx 0.619$ , wherefrom  $D_{\parallel} \approx 0.270 D_0$ , in very good agreement with the experimental data.

It is also interesting to investigate confinement effects on particle sedimentation. To this aim, we have measured the settling speed  $v(\theta)$  of the silica particles by finely adjusting the cell tilt  $\theta$  on the horizontal with the inclinometer. One has  $v(\theta) = v_s^c \sin \theta$ , where  $v_s^c$  is the settling speed a particle would acquire if the confining cell were set vertically. By comparing  $v_s^c$  with the “unconstrained” Stokes speed  $v_s = m^* g/f \approx 9 \mu\text{m/s}$ , where  $m^*$  is the particle buoyant mass and  $f = 6\pi\eta a$  the friction coefficient, we found  $v_s^c/v_s \approx 0.24$ , which is quite close to the experimental value for  $D_{\parallel}/D_0$ . Hence, the effects of confinement on sedimentation are found to be very similar to those on diffusion.

### B. Temperature field and particle thermophoretic drift

The radial temperature distribution  $T(r)$  in pure water was obtained by fluorescence thermometry. The inset in Fig. 2 shows that the peak temperature increase  $\Delta T_0 = \Delta T(0)$  induced on the beam axis depends linearly on the incident laser power  $P$  (in W) as  $\Delta T_0 = (87.7 \pm 0.4)P$ . The figure body shows that, when rescaled

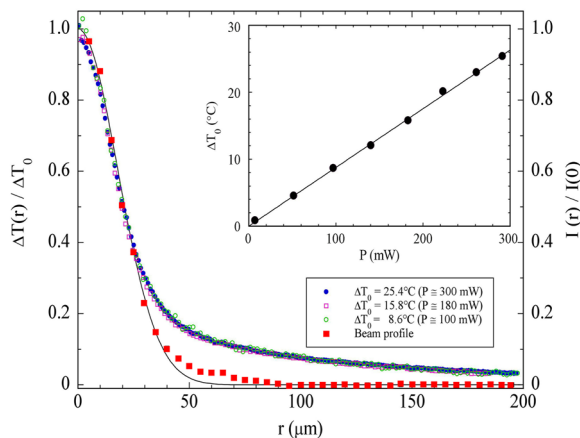


**FIG. 2.** Inset: Peak temperature difference on the optical axis  $\Delta T_0$  as a function of the laser power  $P$ , with the linear fit given in the text. Body: Temperature profiles, scaled to  $\Delta T_0$  obtained in pure water for three values of  $\Delta T_0$ . Plotted on the right axis is the normalized beam profile with a Gaussian fit (full line) corresponding to a beam waist of  $36 \mu\text{m}$  on the sample plane.

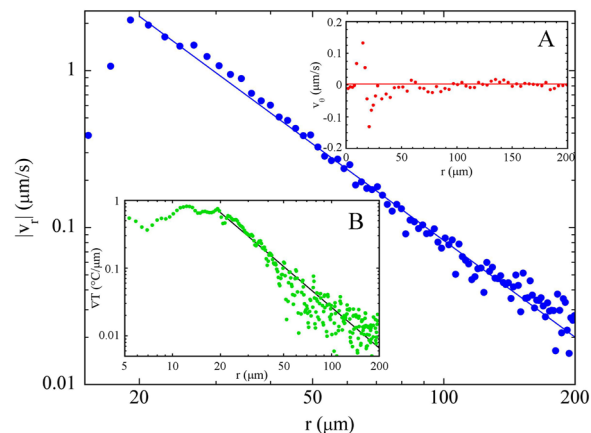


**FIG. 3.** Body: Magnitude of the radial speed  $v_r(r)$  acquired by the silica particles at a surface coverage  $\phi_0 \approx 0.3\%$  for a laser power of about 300 mW, fitted for  $r \geq 20 \mu\text{m}$  as a power law  $|v_r| = v_0 r^{-\beta}$ , with  $\beta = 2.04 \pm 0.08$ . Inset A shows that, after correction for residual drifts, the tangential component of the velocity is fully negligible. Inset B: Thermal gradient  $\nabla T(r)$  obtained as the numerical derivative of the temperature profile for  $\Delta T_0 = 25.4^\circ\text{C}$ . The full line is a power-law fit  $\nabla T(r) = Cr^{-2}$ .

to  $\Delta T_0$ , the whole temperature profiles nicely superimpose. For  $r \lesssim 25 \mu\text{m}$  these profiles approximately superimpose with the IR beam profile, but at larger distance from the optical axis they display a long exponential tail with a decay constant of about  $100 \mu\text{m}$ , so that even at the limit of the field of view  $|v_r|$  is still about 3% of its value in the origin.

It is however worth pointing out that, in the presence of the silica particles that *do not* absorb the IR beam, the effectively illuminated volume is reduced by a factor  $f = 1 - \Phi$ . For the initially even particle distribution this just causes a uniform reduction of  $\Delta T(r)$  but, as time goes by, the optothermally-driven particle drift affects the spatial distribution of the temperature field. In particular, the accumulation of a compact cluster around the optical axis leads to a substantial reduction of the temperature increase in the beam spot region with respect to  $\Delta T_0$ . Besides the particles, illuminated from below, act as tiny ball lenses that focus the incident field in the overlying thin solvent layer,<sup>26</sup> introducing small-scale fluctuations in the temperature field that, as we shall see, may affect the crystallization process. In what follows, with  $\Delta T_0$  we shall always indicate the on-axis temperature increase *before* particle accumulation takes place.

When the thermal field is switched on, the silica particles are driven by thermophoresis towards the hot spot, namely they are “thermophilic,” a behavior shared by a rather limited number of colloidal systems<sup>27,28</sup> that is particularly suited to our purposes. Figure 3 shows that the particle drift velocity is strictly radial over the whole field of view. Outside the beam spot (where it rapidly vanishes), the magnitude of  $v_r$  decays to a good approximation as  $r^{-2}$ . Due to the increasing thermophoretic speed, by approaching the beam center the particle trajectories become progressively more ballistic, with a Peclet number  $\text{Pe} = av/D$  that increases from about 1.5 to more than 100 by approaching the beam spot. Writing  $v(r) = -D_T \nabla T(r)$ , one finds a thermophoretic mobility  $D_T \approx (-3.5 \pm 0.2) \mu\text{m}^2 \text{s}^{-1} \text{K}^{-1}$ . It is worth noticing that using thermophoresis as a driving field has

the advantage that, in phoretic motion, particle hydrodynamic interactions are not long-ranged like those encounters for instance in colloid sedimentation, which may substantially influence the crystal nucleation rate.<sup>28</sup>

In principle, however, particle motion could be affected by natural convection of the solvent and, possibly, also by thermo-osmosis, namely by the slip velocity of water along the thermally inhomogeneous cell windows. Due to the very small cell thickness, however, the effect of convection is readily found to be negligible. Indeed, using a lubrication approximation, the convective velocity can be written as  $u_c = (h^3 g \alpha \nabla T(r) / 12 \eta) f(r/z)$ , where  $\eta$  and  $\alpha$  are the solvent viscosity and thermal expansivity, and  $f(r/z)$  is a simple cubic function of the radial distance scaled to the height from the cell bottom that attains a maximum value of about 0.1.<sup>30,31</sup> In our experimental geometry, using from Fig. 2 a maximum temperature gradient  $(\nabla T)_{\text{max}} \sim 2 \text{K}/\mu\text{m}$ , we obtain  $u_c \leq 5 \text{nm s}^{-1}$ . With our closed cell geometry, thermo-osmosis is predicted to involve flows confined to a few correlation lengths about the cell upper and lower silica windows, which should be directed to the colder regions, together with a counter-flow in the bulk of the cell required to ensure zero net mass flow, therefore directed to the hot regions.<sup>32</sup> Since the particles, lying on the cell bottom, are not exposed to the thermo-osmotic flow at the upper plate, the effect of the counter-flow is arguably stronger, adding to thermophoresis in pushing the particles to the hot side. However, how strong is this contribution? To compare thermo-osmosis to thermophoresis as a driving force, we coated the surface of the silica particles with a block copolymer (a poloxamer), which has the effect of switching the particle behavior from thermophilic to thermophobic.<sup>33</sup> By repeating the experiment with the coated particles, the velocity field is reversed, while of course the thermo-osmotic effect would still drive them to the hot side since the cell windows are uncoated. We may then safely

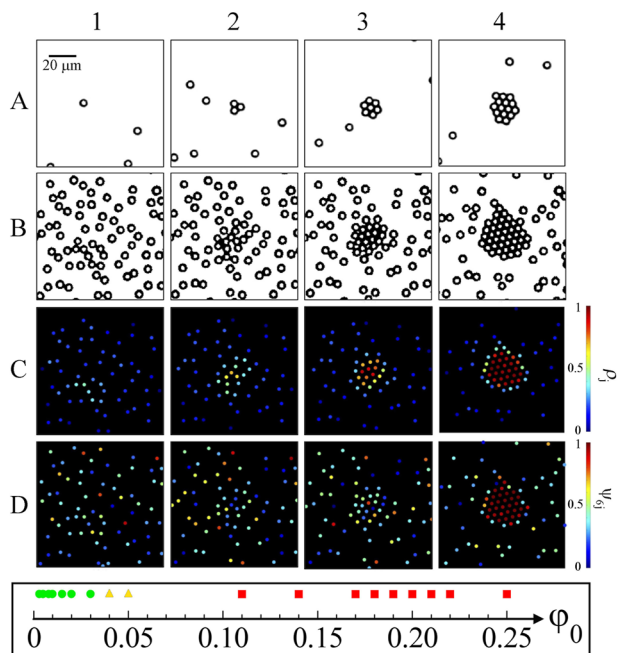


**FIG. 4.** Image sequence of the nucleation process. Panel (a) nucleation and growth for a dilute sample ( $\varphi_0 \approx 1.4\%$ ). Frames  $\{1, 2, 3, 4\}$  correspond to delays after the laser is turned on of  $\{0, 40, 84, 182\}$  s respectively. Panel (b) nucleation occurring for a concentrated sample ( $\varphi_0 \approx 14\%$ ). Frames  $\{1, 2, 3, 4\}$  correspond to delays after the laser is turned on of  $\{0, 4, 6, 16\}$  s respectively. The time-evolution of local density and orientational order parameters  $\rho_j$  and  $\psi_{6j}$  corresponding to the sequence in panel (b) are respectively shown in panels (c) and (d), where the spots, colored according to the scale on the right, are positioned at the particle centroids. All values of  $\varphi_0$  investigated in this work are presented in the box at the figure bottom, which shows those samples that crystallize with no time delay (dots), those where crystal nucleation is apparently preceded by the formation of a dense disordered phase (squares), and those where a time delay, if it exists, is too short to be detected (triangles).

assume that thermo-osmotic effects, if present, are much weaker than thermophoresis.

### C. Crystal nucleation

Figure 3 shows that both the thermal gradient and the thermophoretic velocity basically vanish within the beam spot region, which then acts as a “reservoir” where the particles progressively accumulate generating a dense structure. Visual inspection shows that the growth kinetics of this structure qualitatively changes by increasing the initial particle surface coverage. While at very low  $\varphi_0$  the dense region takes on a hexagonal 2D crystal structure right from the beginning [panel (a) in Fig. 4], at high surface coverage [panel (b)] we first observe the formation of a dense fluid phase that only after a variable lag time evolves into a crystal (see also movie M1 in the supplementary material).

To better characterize the structure of the dense phase, it is worth constructing a Voronoi tessellation of the plane, namely a partition that associates to each particle centroid  $j$  a convex polygon  $\mathcal{V}_j$ , called a Voronoi cell, made of all the points in the plane that are closer to  $j$  than to any other particles. The number of vertices

of a Voronoi cell  $\mathcal{V}_j$  is called the coordination number of particle  $j$ , and coincides in ordered (and quasi-ordered structures like defective crystals) with the number of nearest neighbours. Using the Voronoi tessellation, we can then define two order parameters. The degree of packing can be quantified by defining a local particle density at the position of each particle  $j$  as

$$\rho_j = \frac{\mathcal{A}_{ocp}}{\mathcal{A}_j}$$

where  $\mathcal{A}_j$  is the surface area of the Voronoi cell  $\mathcal{V}_j$  and  $\mathcal{A}_{ocp}$  is the maximal surface area of a cell for a 2D ordered close packing, corresponding to a particle surface coverage  $\varphi_{ocp} = \pi/(2\sqrt{3}) \approx 0.91$  (thus  $0 \leq \rho_j \leq 1$ ).<sup>34,35</sup> The local degree of orientational ordering can instead be judged from the value of the parameter

$$\psi_{6j} = \frac{1}{n} \left| \sum_{k=1}^n \exp(-i6\vartheta_{jk}) \right|$$

where  $n$  is the number of vertices of  $\mathcal{V}_j$  and  $\vartheta_{jk}$  is the angle formed with a reference axis by the line joining the particle centroid with each vertex  $k$ .

While for the experiment at low  $\varphi_0$  shown in panel (a) in Fig. 2 crystallization seems to be immediate, the time evolution of  $\rho_j$  and  $\psi_{6j}$  for the experiment in panel (b), shown in panels (c) and (d), suggests that a substantially dense amorphous phase has to build up before a crystal phase shows up (see also movie M2 in the supplementary material). Notably, ordering takes place quite abruptly, which allows to define rather precisely a time lag  $\Delta t = t_c - t_0$  from the moment  $t_0$  when the laser is turned on and particle accumulation around the beam spot begins, and the moment  $t_c$  when ordering of the accumulated dense phase takes place. The time lag  $\Delta t$  can be gauged by evaluating the average order parameters over those particles that lie, at a given time  $t$ , within the region  $A_c$  occupied by the accumulated particles at the time  $t_c$  when ordering begins,<sup>36</sup>

$$\rho(t) = \langle \rho_j \rangle_{j \in A_c}, \quad \psi_6(t) = \langle \psi_{6j} \rangle_{j \in A_c}.$$

The inset of Fig. 5 shows that this procedure yields a rather well defined value for  $\Delta t$  even when the latter is quite short. Notably, this apparent “two-step” nucleation was detected for *any* values of the on-axis temperature increase  $\Delta T_0$  whenever the initial surface coverage  $\varphi_0 \gtrsim 0.03$ – $0.05$  (see the box at the bottom of Fig. 4). Only for lower values of  $\varphi_0$  compaction and ordering are basically simultaneous, once again regardless of  $\Delta T$ , which nevertheless plays a primary role in controlling the timescale required for crystal nucleation. Figure 5 shows indeed that  $\Delta t$  drops as  $\Delta T^{-\alpha}$  where  $\alpha = 1.15 \pm 0.05$ . In fact,  $\Delta t$  becomes as large as 200 s by reducing  $\Delta T$  to about  $1^\circ\text{C}$ , suggesting that without “thermal forcing” crystal nucleation may even be suppressed. A semi-quantitative argument suggesting that  $\Delta t$  should roughly scale as the inverse of  $\Delta T_0$  is the following. Since the *whole* temperature field  $\Delta T(r)$  scales with  $\Delta T_0$ , both the particle flux and the total number of particles accumulated into the beam spot region at a given time  $t$  should also be proportional to  $\Delta T_0$ . Then, if the minimal average packing density  $\varphi_c$  required to trigger crystal nucleation does not depend on  $\Delta T_0$ , the time  $\Delta t$  to reach  $\varphi_c$  would strictly scale as  $\Delta T_0^{-1}$ . The observed experimental trend then

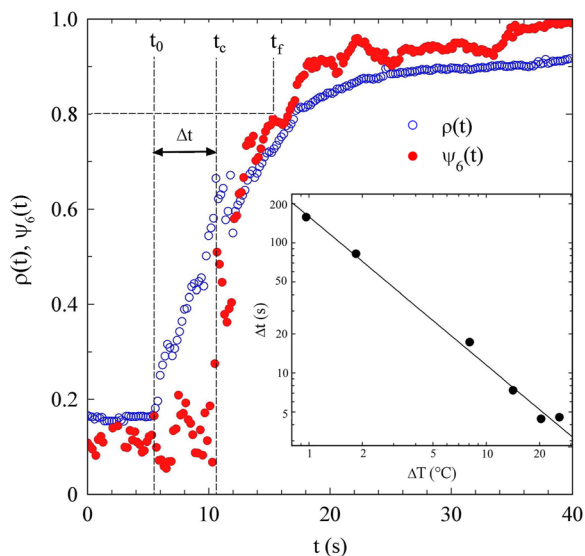


**FIG. 5.** Estimation, made by contrasting the increase of  $\rho(t)$  and  $\psi_6(t)$  with respect to their initial values, of the time interval  $\Delta t$  before crystal nucleation starts at  $\varphi_0 = 0.14$  [corresponding to  $\rho(0) \approx 0.155$ ] for a temperature increase  $\Delta T \approx 25^\circ\text{C}$  (which yields the shortest value of  $\Delta t$ ). The double-log plot in the inset suggests that the dependence of  $\Delta t$  on the incident laser power can approximately be fitted by a power law  $\Delta t \propto \Delta T^{-\alpha}$ , with  $\alpha = 1.15 \pm 0.05$ .

suggests that the “critical” packing fraction at which crystallization starts is substantially independent from  $\Delta T_0$ , namely from the driving force.

To check for this guess, we averaged as before the local surface coverage over the region where particles have accumulated at the time  $t_c$  when the orientational order parameter begins to rise indicating the onset of crystallization. The upper panel in Fig. 6 shows that  $\rho(t_0)$  does not appreciably depend on the  $\Delta T_0$ , with a mean value of about 0.67 that is definitely within the fluid phase. Actually, this value is about 13% lower than freezing limit, likely because the value of  $\rho_j$  is smaller for those particles lying far from the location in the cluster where crystallization starts. In other words, we have no evidence of dynamically arrested precursors of crystal with a homogeneous hexagonal order, namely we cannot speak of a real “two-step” crystallization mechanism but just of the ordering of a 2D-fluid. The lower panel in Fig. 6 shows that, if we conventionally define a moment when ordering has reached completion as the time  $t_f$  when the average orientational order parameter has reached a value  $\psi_6(t_f) \approx 0.8$ ,<sup>20,37</sup> the value of  $\rho(t_f)$  is again basically independent of  $\Delta T_0$ , with an average value  $\rho(t_f) \approx 0.82$  that is well within the crystal phase.

The previous conclusions can be further strengthened by comparing the number of particle  $N_\rho(t)$  in the cluster that have a local density parameter  $\rho_j \geq \rho_c$ , where  $\rho_c \approx 0.79$  is the lower limit of the crystal phase, with the number of particles  $N_\psi(t)$  for which, at the same time  $t$ ,  $\psi_{6j} \geq 0.8$ . The plot in Fig. 7 shows that  $N_\psi(t) \approx N_\rho(t)$  with good approximation, which means that overcoming the freezing line leads to orientational ordering too.

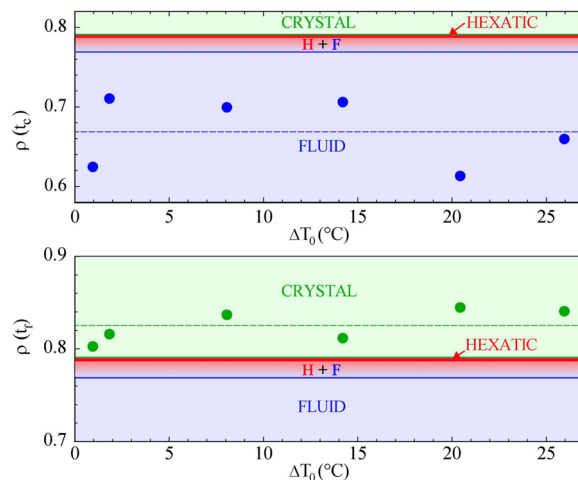


**FIG. 6.** Upper panel: Mean surface density  $\rho(t_0)$  evaluated as in Fig. 5 at the time  $t_c$  when the orientational order parameter  $\psi_6$  starts to increase, plotted on the (scaled) theoretical phase diagram for Hard Disks<sup>38</sup> showing the boundaries of the fluid, hexatic, and crystal phases. Lower panel: Mean surface density  $\rho(t_f)$  evaluated at the time  $t_f$  when  $\psi_6$  reaches a threshold value of 0.8. The dashed lines indicate the mean values of  $\rho(t_c) \approx 0.67$  and  $\rho(t_f) \approx 0.82$  [corresponding to  $\varphi(t_c) \approx 0.61$ ,  $\varphi(t_f) \approx 0.75$ ].

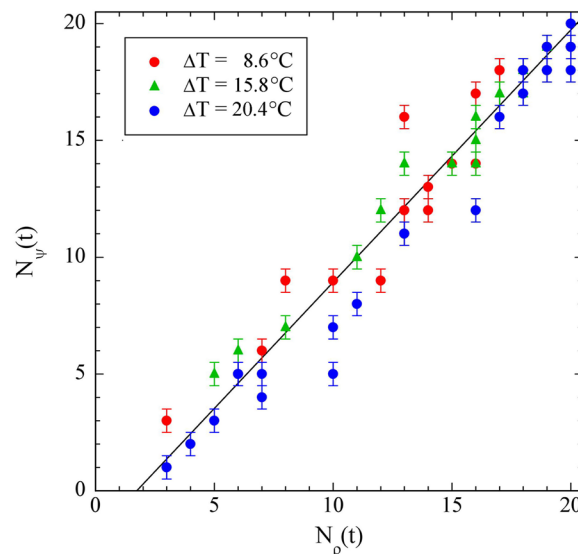


**FIG. 7.** Number of particles  $N_\psi(t)$  in the accumulated cluster whose local orientational parameter exceeds 0.8, vs the number of particles  $N_\rho(t)$  whose surrounding local density exceeds the crystallization limit, plotted for three values of  $\Delta T_0$  shown in the legend and  $\varphi_0 = 0.14$ . The full line is a linear fit to the whole set of data with a slope  $1.07 \pm 0.02$ .

#### D. Crystal growth kinetics

The growth kinetics of the crystallites for  $t \geq \Delta t$ , when the size of the crystallite rapidly becomes comparable or larger than the beam spot size  $w$ , is shown in Fig. 8. The figure shows that

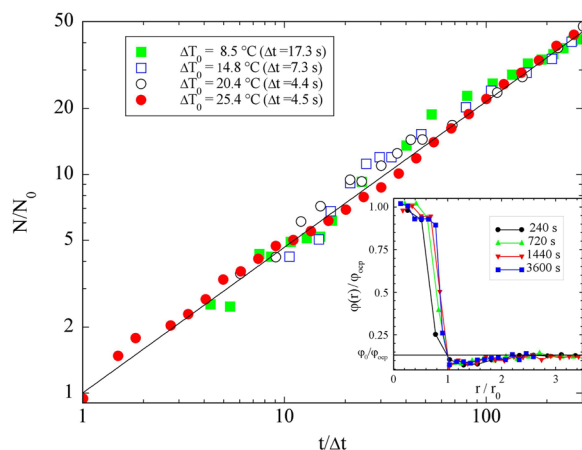


**FIG. 8.** Number of particles in a crystallite,  $N(t)$ , normalized to its value  $N_0$  in the beam spot size at  $t = \Delta t$  for an initial surface coverage  $\phi_0 \approx 0.18$  at four values of  $\Delta T_0$ , with the corresponding value of  $\Delta t$  from Fig. 5. The time evolution of  $N(t)$  is well approximated by  $N(t)/N_0 = (t/\Delta t)^{2/3}$  (full line). Inset: Scaled density profile  $\phi(r)/\phi_{\text{rcp}}$  of a growing crystallite at several growing times. The distance  $r$  from the center is scaled to its value where  $\phi(r) = \phi_0$ .

the growth in time of the number of particles  $N(t)$  contained in a crystallite is accurately described by  $N(t)/N_0 = (t/\Delta t)^{2/3}$  with no fit parameters, where  $N_0$  is the number of particles contained in a crystallite of size  $w$ . Surprisingly, this time trend coincides with the diffusion-limited growth of the average crystal radius in spontaneous 2D Ostwald ripening.<sup>39</sup> Yet this result is probably fortuitous, and just related to the peculiar  $r$ -dependence of the thermophoretic speed. Indeed, when the crystallite reaches and exceeds the beam spot size, we can tentatively assume that its temperature is approximately uniform, but with a markedly reduced average temperature increase  $\Delta T' \sim (1 - \phi_{\text{ocp}})\Delta T \sim 0.1\Delta T$ . Nevertheless, in the region surrounding the growing nucleus, where the particle surface density is still of the order of  $\phi_0$ , the temperature field can be assumed to be weakly disturbed by the presence of the particles. An evaluation of the particle in-flux easily yields  $dN(t)/dt = (2\phi_0/a^2)rv(r) \propto 1/r$  because, from Fig. 3, the thermophoretic speed approximately scales as  $r^{-2}$ . Since the radius of the growing cluster scales as  $r \propto \sqrt{N(t)}$ , it is then immediate to show that, within this simplified model, the number of particles in a crystallite has to grow as  $t^{2/3}$ .

The inset in Fig. 8 highlights a further similarity with the Ostwald ripening process, namely the occurrence of a “depletion region” around a growing crystallite that has been revealed and extensively investigated in inorganic<sup>40</sup> and protein<sup>41</sup> crystal growth, or around the fractal aggregates generated by diffusion-limited colloidal aggregation.<sup>42</sup> Notably, the inset shows that, when the radial coordinate  $r$  is scaled to the crystal size, defined as the value  $r_0$  where  $\phi(r)$  comes down to the initial surface coverage  $\phi_0$ , the depletion regions at several growing times nicely superimpose, while the crystal density profile becomes progressively steeper. The origin of this depletion region is due to consistent growth (as the inverse square of the distance) of the thermophoretic velocity by approaching the crystal border. Therefore, the influx of particles that lie further from the

crystal border does not suffice to replace those that are driven to the interface from a closer position, generating a depleted zone that is easily spotted in movie M3 of the supplementary material. It is finally worth noticing that, if a particle would stick to the crystal as soon as it reaches the interface, the value of  $\phi(r)$  at contact should actually vanish.<sup>43</sup> That the observed value is small but still finite implies that it takes some time for a particle to settle to its final position in the crystal is arguably a further sign of the “fluidized” state of the crystal interface discussed in Sec. III E.

### E. Crystal uniformity

As shown in Fig. 9, the large crystals obtained at late growth stage always have a single-grain structure<sup>44</sup> and display a remarkably small number of lattice defects. Moreover, these few defects are usually located in the crystal core, originating from the rapid ordering of the dense fluid precursor, while the outlying regions are almost defect free. It is actually rather surprising that the incoming particles find their “correct” position without generating point defects, even of they impact on the crystal border at high Peclet number. A clue to figure out the origin of this self-ordering effect is that, as highlighted by movie M3 in the supplementary material, the border region of the growing crystal is somehow “fluidized.” Namely, the incoming particles diffuse and bounce quite a bit, often displacing other particles, before they reach their rest place. In a way, this mechanism may resemble the surface enhanced mobility credited to be at the roots of the origin of ultra-stable glasses in physical vapor deposition methods made both in the lab<sup>45</sup> and *in silico*.<sup>46</sup> Good quality 2D crystals of hard spheres, which are promising for applications in photonics,<sup>1,47</sup> can actually be obtained by other methods,<sup>48–50</sup> sometimes also involving the presence of thermal gradients.<sup>51</sup> Yet, compared to them, optothermal crystallization using a laser is simpler, highly controllable, and, above all, much less time consuming. A further advantage in inducing crystallization by exploiting phoretic effects is arguably the much lesser role played by hydrodynamic fluctuations that are small and with a finite range, while for “real” external field like gravity they are huge and unbounded. Although we cannot present here a systematic study, we have indeed clear evidence in particle sedimentation crystal nucleation is fully frustrated for values of the particle Peclet number that are far smaller than those used in the present study.

### F. Crystal melting

Investigating the kinetic of melting of 2D crystals is probably the most direct strategy to detect the occurrence the rather elusive hexatic phase predicted by the KTHNY theory<sup>3</sup> that, as shown in Fig. 6, takes up only a very narrow region in the phase diagram of hard disks. As mentioned in the introduction, clear and detailed evidence of the existence of a transient hexatic order upon melting has been obtained by Han *et al.*<sup>16</sup> by exploiting soft spheres with a tunable size. This allows huge single crystals to be assembled and then melted by slowly increasing temperature, following the structural evolution of the system. More recently, Thorneywork *et al.*<sup>52</sup> managed to obtain with an ingenious sedimentation experiment the full phase diagram and the equation of state of 2D-confined hard spheres, confirming the existence of an equilibrium hexatic phase



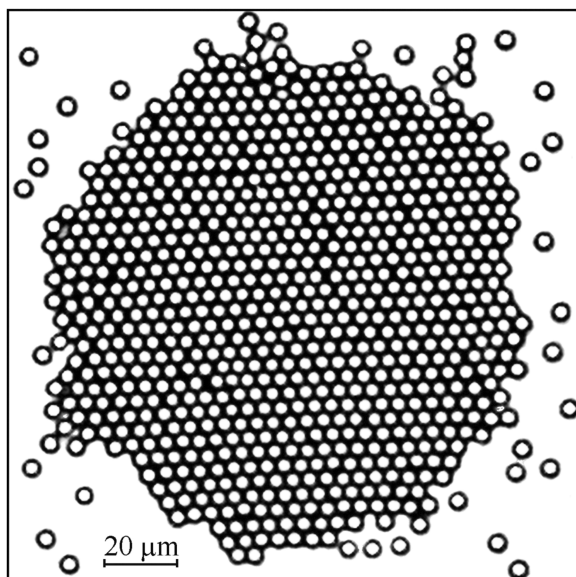


**FIG. 9.** A large 2D crystal, including about 800 particles, obtained from a suspension at  $\phi_0 \approx 0.18$  at a growth time of about 1/2 h.

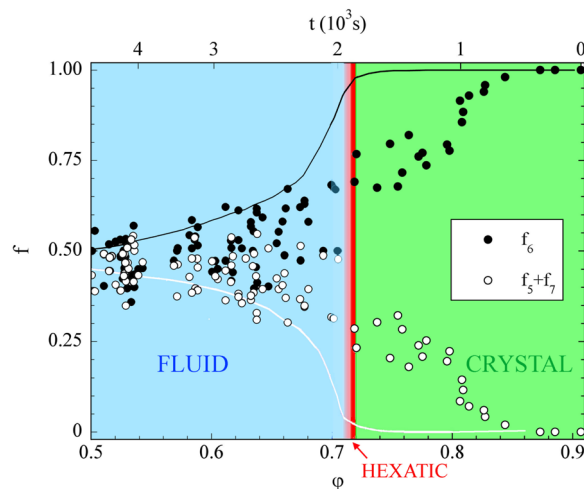


**FIG. 10.** Fraction  $f_6$  of particles that have coordination number  $\nu = 6$  neighbours (full dots) and either  $\nu = 5$  or  $\nu = 7$ ,  $f_5 + f_7$  (open dots), vs the average surface coverage  $\phi$  at a given time, plotted on the phase diagram for hard disks as in Fig. 6. The actual timescale is shown on the upper axis (which runs from right to left). The black and white full linear are numerical result by Kumar and Kumaran<sup>56</sup> obtained by NVE (microcanonical) MC simulations at 50% success rate (namely, the amplitude of the random trial displacement is adjusted such that 50% of the trials lead to non overlapping configurations).

showing at the same time that the crystal/hexatic transition is not, as originally suggested, first order.

The size of the crystallites we obtained is far too small to allow a quantitative study of the evolution of translational/orientational correlations, or of the structure factor of the system, which are necessary to rigorously tell a short-range translational from a quasi-long orientational order. Although we did detect some evidence of the pathway to 2D melting predicted by the KTHNY theory (in particular the unbinding of dislocation pairs), our data statistics is too poor to add solid evidence to the accurate investigation made for soft repulsive spheres.<sup>16</sup> Nevertheless, we regard it as useful to provide some quantitative data on the evolution of structural defects upon melting. Defining as commonly done<sup>53</sup> the coordination number  $\nu$  of a particle as the number of sides of the associated Voronoi tile (which in a fully ordered structures coincides with the number of nearest neighbours), we recall that in the KTHNY route to melting a key role is played by the formation, followed by unbinding, of dislocation pairs, where each dislocation is in turn constituted by pairing a “positive” and a “negative” disclination, respectively corresponding to particles with  $\nu > 6$  and  $\nu < 6$ , typically (but not exclusively)  $\nu = 5$  and  $\nu = 7$ .

Figure 10, which refers specifically to the melting of the crystallite shown in Fig. 9, shows that the fraction of particles with  $\nu = 5$  or  $\nu = 7$ , practically absent in the original crystal, rapidly grows becoming at melting about 1/3 of the particles with a fully ordered local environment ( $\nu = 6$ ), and no apparent discontinuity is detected in this trend when the average surface density  $\phi$  reaches the value predicted for the transition to the hexatic phase. Notably, in the fluid phase  $\langle f_6 \rangle$  is rather close to  $f_6$ , with average values over the whole fluid phase  $\langle f_6 \rangle \approx 0.51$  and  $\langle f_5 + f_7 \rangle \approx 0.43$ . While the result for  $\langle f_6 \rangle$  just confirms within experimental errors what is expected from Euler’s

formula for polyhedra, the result for  $\langle f_5 + f_7 \rangle$  means that the distribution of the coordination number in a dense fluid is very narrow, with almost 95% of the particles having  $\nu \in [5, 7]$ . To compare, in the dilute limit (Poisson-Voronoi tessellation) one has  $f_6 \approx 0.295$ ,  $f_5 \approx 0.259$ ,  $f_7 \approx 0.199$ , which altogether yields just about 75% of the cells,<sup>54,55</sup> mostly due to a strong reduction of the number of particles with  $\nu = 6$ . We are not aware of any other experimental study of the distribution of coordination number in a dense fluid of hard disks, but numerical simulations by (microcanonical) Montecarlo have been presented.<sup>56</sup> Figure 10 compares our experimental data with the simulation results shown in Figs. 6 and 7 of the numerical investigation by Kumar and Kumaran.<sup>56</sup> Although the growth of the number of defects of the crystal upon melting seems to take place earlier than predicted, the experimental and simulation results for the fluid phase are very similar.

#### IV. DISCUSSION AND CONCLUSIONS

The main evidence presented in this work is that the disorder clusters that precede the formation of 2D crystallites have an average surface density that is close but still below the upper limit for the fluid phase. Thus, at variance with previous claims,<sup>19,20</sup> we cannot speak of a true “two-step” nucleation, by which it is commonly meant the formation of a metastable amorphous phase before ordering, but rather of simple field-driven accumulation until the freezing surface density is locally reached. It is still a bit surprising that no accumulation time is apparently required at very low (few percent) initial coverage  $\phi_0$  regardless of the strength of the forces that drives particle accumulation, while one would intuitively expect the particle inward flux to be the key parameter.

Notably, the thermophoretic accumulation in a truly bidimensional cell rapidly yields large uniform 2D-crystals with a tiny number of defects. As discussed in Sec. III E, this is arguably due to the annealing effect due to the fluidization of the outer crystallite regions. The approach we used may then be promising for applications in photonics.

Finally, we have investigated the evolution of the Voronoi tessellation of a melting crystallite, focusing progressive increase of defects and showing that the distribution of the particle coordination number in a dense fluid is very narrow, a result that, although supported by simulation, is anything but obvious.

## SUPPLEMENTARY MATERIAL

Movie M1: Crystal nucleation for a sample at  $\varphi_0 \approx 0.14$ .  
Movie M2: Comparison of the time-evolution of the local density and orientational order parameters for a sample at  $\varphi_0 \approx 0.14$ .  
Movie M3: Late stage growth of a crystal from a suspension at  $\varphi_0 \approx 0.18$ .

## ACKNOWLEDGMENTS

We are extremely grateful to Nitto Italia Srl for the kind gift of the ultrathin double tape used in the 2D cell setup, and we thank S. Buzzaccaro for help in designing the experimental system and for useful discussions.

## AUTHOR DECLARATIONS

### Conflict of Interest

The authors have no conflicts to disclose.

## Author Contributions

**Vincenzo Ruzzi:** Conceptualization (equal); Data curation (equal); Investigation (equal); Writing – original draft (equal). **Jacopo Baglioni:** Data curation (supporting); Investigation (equal); Software (equal); Visualization (equal). **Roberto Piazza:** Conceptualization (lead); Formal analysis (lead); Methodology (equal); Resources (lead); Supervision (lead); Writing – original draft (lead).

## DATA AVAILABILITY

The data that support the findings of this study are available from the corresponding author upon reasonable request.

## REFERENCES

- Z. Cai, Z. Li, S. Ravaine, M. He, Y. Song, Y. Yin, H. Zheng, J. Teng, and A. Zhang, “From colloidal particles to photonic crystals: Advances in self-assembly and their emerging applications,” *Chem. Soc. Rev.* **50**, 5898–5951 (2021).
- J. Zhang, Y. Li, X. Zhang, and B. Yang, “Colloidal self-assembly meets nanofabrication: From two-dimensional colloidal crystals to nanostructure arrays,” *Adv. Mater.* **22**, 4249–4269 (2010).
- J. M. Kosterlitz, “Kosterlitz–Thouless physics: A review of key issues,” *Rep. Prog. Phys.* **79**, 026001 (2016).

- U. Gasser, “Crystallization in three- and two-dimensional colloidal suspensions,” *J. Phys.: Condens. Matter* **21**, 203101 (2009).
- D. Gebauer, M. Kellermeier, J. D. Gale, L. Bergstrom, and H. Cölfen, “Pre-nucleation clusters as solute precursors in crystallisation,” *Chem. Soc. Rev.* **43**, 2348–2371 (2014).
- P. G. Vekilov, “The two-step mechanism of nucleation of crystals in solution,” *Nanoscale* **2**, 2346–2357 (2010).
- T. Palberg, “Crystallization kinetics of colloidal model suspensions: Recent achievements and new perspectives,” *J. Phys.: Condens. Matter* **26**, 333101 (2014).
- J. Russo and H. Tanaka, “The microscopic pathway to crystallization in supercooled liquids,” *Sci. Rep.* **2**, 505 (2012).
- P. R. ten Wolde and D. Frenkel, “Enhancement of protein crystal nucleation by critical density fluctuations,” *Science* **277**, 1975–1978 (1997).
- T. M. Truskett, S. Torquato, S. Sastry, P. G. Debenedetti, and F. H. Stillinger, “Structural precursor to freezing in the hard-disk and hard-sphere systems,” *Phys. Rev. E* **58**, 3083–3088 (1998).
- T. Schilling, H. J. Schöpe, M. Oettel, G. Opletal, and I. Snook, “Precursor-mediated crystallization process in suspensions of hard spheres,” *Phys. Rev. Lett.* **105**, 025701 (2010).
- H. J. Schöpe, G. Bryant, and W. van Megen, “Two-step crystallization kinetics in colloidal hard-sphere systems,” *Phys. Rev. Lett.* **96**, 175701 (2006).
- W. Wöhler and T. Schilling, “Hard sphere crystal nucleation rates: Reconciliation of simulation and experiment,” *Phys. Rev. Lett.* **128**, 238001 (2022).
- J. R. Savage and A. D. Dinsmore, “Experimental evidence for two-step nucleation in colloidal crystallization,” *Phys. Rev. Lett.* **102**, 198302 (2009).
- S. Buzzaccaro, J. Colombo, A. Parola, and R. Piazza, “Critical depletion,” *Phys. Rev. Lett.* **105**, 198301 (2010).
- Y. Han, N. Ha, A. Alsayed, and A. Yodh, “Melting of two-dimensional tunable-diameter colloidal crystals,” *Phys. Rev. E* **77**, 041406 (2008).
- S. van Teeffelen, C. N. Likos, and H. Löwen, “Colloidal crystal growth at externally imposed nucleation clusters,” *Phys. Rev. Lett.* **100**, 108302 (2008).
- A. Caciagli, R. Singh, D. Joshi, R. Adhikari, and E. Eiser, “Controlled optofluidic crystallization of colloids tethered at interfaces,” *Phys. Rev. Lett.* **125**, 068001 (2020).
- K.-Q. Zhang and X. Y. Liu, “*In situ* observation of colloidal monolayer nucleation driven by an alternating electric field,” *Nature* **429**, 739–743 (2004).
- T. H. Zhang and X. Y. Liu, “Multistep crystal nucleation: A kinetic study based on colloidal crystallization,” *J. Phys. Chem. B* **111**, 14001–14005 (2007).
- R. Deng, Y. He, Y. Qin, Q. Chen, and L. Chen, “Measuring pure water absorption coefficient in the near-infrared spectrum (900–2500 nm),” *Natl. Remote Sens. Bull.* **16**, 192–206 (2012).
- J.-Y. Tinevez, N. Perry, J. Schindelin, G. M. Hoopes, G. D. Reynolds, E. Laplanche, S. Y. Bednarek, S. L. Shorte, and K. W. Eliceiri, “TrackMate: An open and extensible platform for single-particle tracking,” *Methods* **115**, 80–90 (2017).
- D. Ross, M. Gaitan, and L. E. Locascio, “Temperature measurement in microfluidic systems using a temperature-dependent fluorescent dye,” *Anal. Chem.* **73**, 4117–4123 (2001).
- A. Goldman, R. Cox, and H. Brenner, “Slow viscous motion of a sphere parallel to a plane wall—I Motion through a quiescent fluid,” *Chem. Eng. Sci.* **22**, 637–651 (1967).
- T. Benesch, S. Yiacoymi, and C. Tsouris, “Brownian motion in confinement,” *Phys. Rev. E* **68**, 021401 (2003).
- In ray optics, these tiny ball lenses would generate a cuspid caustic with a singularity point at about 10  $\mu\text{m}$  over the particle top, hence well above the cell upper coverglass.
- S. Iacopini, R. Rusconi, and R. Piazza, “The ‘macromolecular tourist’: Universal temperature dependence of thermal diffusion in aqueous colloidal suspensions,” *Eur. Phys. J. E* **19**, 59 (2006).
- R. Piazza and A. Parola, “Thermophoresis in colloidal suspensions,” *J. Phys.: Condens. Matter* **20**, 153102 (2008).
- S. Ketzetzi, J. Russo, and D. Bonn, “Crystal nucleation in sedimenting colloidal suspensions,” *J. Chem. Phys.* **148**, 064901 (2018).
- R. Birikh, “Thermocapillary convection in a horizontal layer of liquid,” *J. Appl. Mech. Tech. Phys.* **7**, 43–44 (1966).

- <sup>31</sup>D. Rivière, B. Selva, H. Chraïbi, U. Delabre, and J.-P. Delville, "Convection flows driven by laser heating of a liquid layer," *Phys. Rev. E* **93**, 023112 (2016).
- <sup>32</sup>P. Anzini, Z. Filiberti, and A. Parola, "Fluid flow at interfaces driven by thermal gradients," *Phys. Rev. E* **106**, 024116 (2022).
- <sup>33</sup>This dramatic change of behavior confirms once again that thermophoresis is a purely interfacial effect, namely, it mostly depends on the nature of the particle surface and just marginally on its bulk properties.<sup>56,57</sup>
- <sup>34</sup>J. Russo and H. Tanaka, "Crystal nucleation as the ordering of multiple order parameters," *J. Chem. Phys.* **145**, 211801 (2016).
- <sup>35</sup>S. Torquato, "Nearest-neighbor statistics for packings of hard spheres and disks," *Phys. Rev. E* **51**, 3170 (1995).
- <sup>36</sup>Note that the average surface density at time  $t$  is then related to  $\rho(t) = \langle \rho_j \rangle_{j \in A}$  by  $\varphi(t) \simeq 0.91\rho(t)$ . To obtain a fair average it is however important, in particular for small clusters, to exclude those particles that lie on the border, to which cannot be associated a Voronoi cell.
- <sup>37</sup>V. W. De Villeneuve, R. P. Dullens, D. G. Aarts, E. Groeneveld, J. H. Scherff, W. K. Kegel, and H. N. Lekkerkerker, "Colloidal hard-sphere crystal growth frustrated by large spherical impurities," *Science* **309**, 1231–1233 (2005).
- <sup>38</sup>M. Engel, J. A. Anderson, S. C. Glotzer, M. Isobe, E. P. Bernard, and W. Krauth, "Hard-disk equation of state: First-order liquid-hexatic transition in two dimensions with three simulation methods," *Phys. Rev. E* **87**, 042134 (2013).
- <sup>39</sup>J. H. Yao, K. R. Elder, H. Guo, and M. Grant, "Ostwald ripening in two and three dimensions," *Phys. Rev. B* **45**, 8173–8176 (1992).
- <sup>40</sup>G. Banfi, V. Degiorgio, A. R. Rennie, and J. G. Barker, "Small-angle neutron scattering study of crystal growth in semiconductor-doped glasses," *Phys. Rev. Lett.* **69**, 3401–3404 (1992).
- <sup>41</sup>A. McPherson, A. J. Malkin, Y. G. Kuznetsov, S. Koszelak, M. Wells, G. Jenkins, J. Howard, and G. Lawson, "The effects of microgravity on protein crystallization: Evidence for concentration gradients around growing crystals," *J. Cryst. Growth* **196**, 572–586 (1999).
- <sup>42</sup>M. Carpineti, M. Giglio, and V. Degiorgio, "Mass conservation and anticorrelation effects in the colloidal aggregation of dense solutions," *Phys. Rev. E* **51**, 590–596 (1995).
- <sup>43</sup>F. Sciortino and P. Tartaglia, "Structure factor scaling during irreversible cluster-cluster aggregation," *Phys. Rev. Lett.* **74**, 282–285 (1995).
- <sup>44</sup>The absence of polycrystallinity is because crystallization always starts from a single point within the cluster. We never observe multiple nucleation within an aggregate.
- <sup>45</sup>S. F. Swallen, K. L. Kearns, M. K. Mapes, Y. S. Kim, R. J. McMahon, M. Ediger, T. Wu, L. Yu, and S. Satija, "Organic glasses with exceptional thermodynamic and kinetic stability," *Science* **315**, 353–356 (2007).
- <sup>46</sup>S. Singh, M. Ediger, and J. J. De Pablo, "Ultrastable glasses from *in silico* vapour deposition," *Nat. Mater.* **12**, 139–144 (2013).
- <sup>47</sup>R. Borah, A. Karthick Raj, A. C. Minja, and S. W. Verbruggen, "A review on self-assembly of colloidal nanoparticles into clusters, patterns, and films: Emerging synthesis techniques and applications," *Small Methods* **7**, 2201536 (2023).
- <sup>48</sup>B. Van Duffel, R. Ras, F. De Schryver, and R. Schoonheydt, "Langmuir–Blodgett deposition and optical diffraction of two-dimensional opal," *J. Mater. Chem.* **11**, 3333–3336 (2001).
- <sup>49</sup>J.-T. Zhang, L. Wang, D. N. Lamont, S. S. Velankar, and S. A. Asher, "Fabrication of large-area two-dimensional colloidal crystals," *Angew. Chem., Int. Ed.* **51**, 6117–6120 (2012).
- <sup>50</sup>J. Sun, C.-J. Tang, P. Zhan, Z.-L. Han, Z.-S. Cao, and Z.-L. Wang, "Fabrication of centimeter-sized single-domain two-dimensional colloidal crystals in a wedge-shaped cell under capillary forces," *Langmuir* **26**, 7859–7864 (2010).
- <sup>51</sup>X. Sun, Y. Li, T. H. Zhang, Y.-Q. Ma, and Z. Zhang, "Fabrication of large two-dimensional colloidal crystals via self-assembly in an attractive force gradient," *Langmuir* **29**, 7216–7220 (2013).
- <sup>52</sup>A. L. Thorneywork, J. L. Abbott, D. G. Aarts, and R. P. Dullens, "Two-dimensional melting of colloidal hard spheres," *Phys. Rev. Lett.* **118**, 158001 (2017).
- <sup>53</sup>D. R. Nelson and F. Spaepen, "Polytetrahedral order in condensed matter," *Solid State Phys.* **42**, 1–90 (1989).
- <sup>54</sup>R. E. Miles and R. J. Maillardet, "The basic structures of Voronoi and generalized Voronoi polygons," *J. Appl. Probab.* **19**, 97–111 (1982).
- <sup>55</sup>P. Calka, "An explicit expression for the distribution of the number of sides of the typical Poisson-Voronoi cell," *Adv. Appl. Probab.* **35**, 863–870 (2003).
- <sup>56</sup>V. S. Kumar and V. Kumaran, "Voronoi neighbor statistics of hard-disks and hard-spheres," *J. Chem. Phys.* **123**, 074502 (2005).